New Electric Double-Layered Magnetic Fluids Based on Copper, Nickel, and Zinc Ferrite Nanostructures

Marcelo Henrique Sousa and Francisco Augusto Tourinho

Complex Fluids Group - Instituto de Química - Universidade de Brasília, CP 04478, 70919-970 Brasília (DF), Brazil

Jérôme Depeyrot,* Geraldo José da Silva, and Maria Cristina F. L. Lara

Complex Fluids Group - Instituto de Física - Universidade de Brasília, CP 04455, 70919-970 Brasília (DF), Brazil

Received: October 24, 2000

We report on stable colloidal aqueous suspensions of magnetic nanostructures made of copper, nickel, and zinc ferrites. These magnetic fluids could represent a new alternative for biological applications. The basic steps of the nanoparticles synthesis, their chemical surface treatment, and their peptization in a stable colloidal sol are given. Their chemical composition is carefully checked, and X-ray diffraction patterns provide both their mean size and a structural characterization. Magnetization results obtained at 300 K are presented and discussed.

Introduction

Stable colloidal suspensions of nanosized magnetic particles, ferrofluids, or magnetic fluids are a topic of great interest, since they give rise to numerous technological applications due in part to the versatility of molecular carrier liquids such as polar and non polar media.[1] Fundamental studies are generally performed in electric double-layered magnetic fluids[2] (EDL-MF), as they exhibit many interesting properties when easily variable parameters such as concentration, pH, or ionic strength are changed.[3] In the very near future, a promising development for magnetic fluids applied technology will be their use in biological purposes. Recently, biocompatible magnetic fluids (B-MF) based on maghemite (γ-Fe_2O_3) nanoparticles has been successfully grafted by antibodies[4,5] in order to transport them inside different human tissues. Nevertheless, in human blood, the titration of maghemite, which is an iron ferrite, is difficult, as their iron atoms are mixed with the hemoglobin ones. The synthesis of magnetic fluids based on other metal ferrites could therefore mean a new alternative to performing biological in vivo experiments, as they would be notably easier to titrate. Very recently, the suitability of nickel ferrite particles for optical titration in biological applications has been checked.[6]

Spinel ferrite type particles (MFe_2O_4, where M is a *d*-block metal—Mn, Fe, Co, Ni, Cu, and Zn) are preferentially used because of their nonoxydability and their significant magnetization compared to other metallic magnetic particles.[7] To our knowledge, only the chemical synthesis of EDL-MF based on iron, cobalt, manganese,[8] mixed zinc−manganese magnetic ferrites, and zinc nonmagnetic ferrite[9] has been reported until now.

We present in this work and, for the first time in the literature, a preparation process of three new aqueous EDL-MFs based on copper, nickel, and zinc (magnetic) ferrites. The chemical composition of our nanoparticles is checked using chemical analysis methods and measurements of the magnetic material yield. Then X-ray diffraction measurements are performed in order to investigate the crystalline structure and to provide a mean diameter of our magnetic particles. Finally, magnetization measurements obtained for the three kinds of EDL-MF samples, are presented and discussed.

Experimental Section

A. Reagents. All the reagents used in this work are products of analytical purity. Nitrogen was passed through both prepared solutions and distilled water before its use in order to avoid air contamination.

B. EDL-MF Synthesis. In a past few years, chemical preparation of nonsurfacted aqueous magnetic fluids based on spinel ferrite particles has been proposed by Massart,[10] the synthesized product being called at that time ionic MF. Very recently,[2] we introduced a more realistic term, such as electric double-layered magnetic fluids (EDL-MF), in reference to the mechanism used for particle peptization, as in the case of surfacted magnetic fluids (S-MF). In the chemical synthesis of EDL-MF, fine particles of magnetic oxide are directly precipitated out and then peptized using an appropriated particle surface treatment, which, in aqueous media, leads to electrostatic repulsion between them. In this case, the electric charges provided by the proton equilibrium at the interface particle/solution introduce intense enough repulsive forces between the particles to avoid their aggregation and to allow the formation of a stable EDL-MF. In such model, the oxide particles can be seen as a diprotic weak acid, being therefore charged negatively ($S-O^-$), neutral (S−OH), and positively ($S-OH_2^+$) in alkaline, weakly acidic, and acidic media, respectively.

The preparation process of ferrofluids needs three basic steps: first, the particle synthesis, then the chemical surface treatment, and finally, the peptization of the particles in a stable colloidal solution.

* Corresponding author. Fax: +55-61-307-23-63. E-mail address: depeyrot@fis.unb.br.

10.1021/jp0039161 CCC: $20.00
Published on Web 01/20/2001

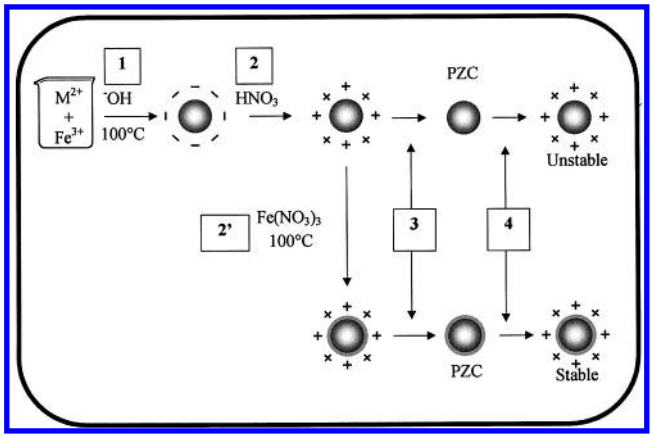

Figure 1. General scheme of the synthesis for our acidic EDL-MF based on nickel, copper, and zinc ferrites. M^{2+} means Ni^{2+}, Cu^{2+}, or Zn^{2+}, and PZC means point of zero charge.

Magnetic particles of ferrofluids must be chemically stable in the liquid carrier and must have a convenient size to provide colloidal sols.[11] In the case of magnetite, the suitable particle diameters are on the order of a few nanometers. Since copper, nickel, and zinc ferrites have approximately the same density as that of magnetite (5.39 g cm^{-3}), this size range is also convenient for these three kinds of ferrites.

The synthesis of ultrafine copper, nickel, and zinc ferrite particles is already known.[12] Nevertheless, to our knowledge, the elaboration of magnetic fluids based on such nanoparticles has not been yet performed. In the following, a procedure of such aqueous EDL-MF preparation is described and carried out (see Figure 1).

Particle Synthesis (step 1 in Figure 1). $CuFe_2O_4$, $NiFe_2O_4$, and $ZnFe_2O_4$ oxide particles were prepared using hydrothermal coprecipitating aqueous solutions of $CuCl_2-FeCl_3$, $NiCl_2-FeCl_3$, and $ZnCl_2-FeCl_3$ mixtures, respectively, in alkaline medium, as described by the schematic reaction

$$M^{2+} + 2Fe^{3+} + 8\,^{-}OH \rightarrow MFe_2O_4 + 4H_2O \qquad (1)$$

Moreover, the synthesis does not occur at room temperature, and the reagents have to be brought to a boil. Since both the particle size and the initial surface (chemically active) state are determined by the coprecipitation procedure, it is therefore necessary to control the relative supersaturation during the synthesis process. This can be achieved mainly by monitoring the following parameters:[8,13]

(i) The starting concentration in metal solution; here, a 2:1 volume mixture of $FeCl_3$ 0.5 mol L^{-1} and MCl_2 0.5 mol L^{-1} (with M = Ni^{2+}, Cu^{2+}, or Zn^{2+}) according to the stoichiometry of the schematic reaction [eq 1].

(ii) The coprecipitation temperature, which must be 100 °C, as previously said.

(iii) The initial $Fe^{3+}-M^{2+}$ mixture acidity to avoid a possible metal hydrolysis before the base addition.

(iv) The way of mixing the different reagents; the $Fe^{3+}-M^{2+}$ mixture must be quickly poured into the alkaline medium under vigorous stirring.

(v) The nature and concentration of the base; here, NaOH 1 mol L^{-1}.

Surface Treatment and Peptization. After the coprecipitation step, the colloidal size of the particles is not sufficient to keep them in suspension. A sluggish precipitate is formed, and even after it is washed, the high ionic strength of the medium plays a screening effect and does not permit sufficient repulsion between the particles. To suppress this screening effect, one has to wash out the ion excess, so the particle surface is therefore cleaned by a (2 mol L^{-1}) HNO_3 solution (step 2 in Figure 1). Afterward, the system therefore becomes acidic and the particles positively charged. As the NO_3^- counterions are nonflocculating ones, it is possible, by passing before the point of zero charge (PZC, steps 3 and 4 in Figure 1), to obtain a colloidal sol after centrifugation and the addition of a minimum amount of water. Such acidic sols directly obtained after the washing process are not longer thermodynamically stable. The copper, nickel, and zinc ferrite particles are progressively destroyed in acidic medium. To improve the procedure in order to prevent the particles from the acidic attack, we have proposed an empirical process:[14] after nitric acid treatment, the precipitate is boiled with a 0.5 mol L^{-1} $Fe(NO_3)_3$ solution and kept boiling for half an hour (step 2' in Figure 1). Then the acidic EDL-MF synthesis occurs, probably due to the formation on the particle surface of a shell of amorphous ferric hydroxides with a high chemical stability, the solubility constant being about 10^{-38}. Recent results of Raman Spectroscopy experiments, performed on EDL-MF samples based on $ZnFe_2O_4$ nanoparticles, enhanced this previous interpretation.[15]

C. Synthesis Characterization. Once the EDL-MF synthesis has been performed, one has to verify the nature of the synthesized material and to know the particles amount in solution, which is proportional to the total concentration in metal. In this way, our samples composition has been controlled by both chemical analysis and measurements of the magnetic material yield.

Titrations. Suitable titrations were performed for our three types of ferrofluid samples based on $CuFe_2O_4$, $NiFe_2O_4$, and $ZnFe_2O_4$ ferrites. Iron (III) titration was performed by dichromatometry and copper (II) titration by volumetric analysis with iodine; nickel (II) titration was quantified by gravimetric analysis with dimethylglioxime, and zinc (II) titration was determined using plasma emission spectroscopy.

Magnetic Material Yield. The experimental procedure used here to determine the particle stoichiometry and the best value in molar fraction between M^{2+} and Fe^{3+} is an adaptation of the method of continuous variation, or "Job's method".[16] For the three kind of samples, a series of solutions of equal total concentration in metal [$M^{2+} + Fe^{3+}$] has been prepared in each solution, with different relative amounts of M^{2+} and Fe^{3+} reacting in excess of sodium hydroxide in order to obtain the ferrite nanoparticles. For each solution, the corresponding magnetic material yield was measured using the Gouy method.[17] In this experiment, due to the force acting on a magnetic sample when submitted to a magnetic field gradient, an apparent increase in mass Δm can indeed be detected when the field is turned on, using an improved magnetic balance. It was therefore possible to obtain for all our synthesized nanoparticles the variations of the magnetic material yield, proportional to Δm, as a function of the divalent metal molar ratio.

D. Structural Characterization and Particle Size Determination Using X-Ray Diffraction Experiments. To determine both the crystalline structure of our synthesized nanoparticles and their respective mean diameters, we realized X-ray diffraction experiments on a powder obtained after evaporating the liquid carrier of the samples. Our measurements were performed on such polycrystalline samples by using an X-ray difractometer installed in a conventional Rigaku/Geigerflex generator operating at 40 kV/30 mA, and the Cu$-K\alpha$ radiation was selected by a graphite monochromator at $\lambda = 1.54$ Å.

TABLE 1: EDL-MF Samples Characteristics: Molar Concentration (C_M), Ionic Strength (C_S), Volume Fraction of Nanomaterial (ϕ), Number of Particles per Cubic Centimeter (n) and Mean Distance between Particles Compared to the X-ray Size (D_{pp}/D_{XR})

			$NiFe_2O_4$			$CuFe_2O_4$			$ZnFe_2O_4$		
	C_M (mol L^{-1})	C_s (mol L^{-1})	ϕ (%)	n ($10^{16}cm^{-3}$)	D_{pp}/D_{XR}	ϕ (%)	n ($10^{16}cm^{-3}$)	D_{pp}/D_{XR}	ϕ (%)	n ($10^{16}cm^{-3}$)	D_{pp}/D_{XR}
A	0.50	0.40	0.75	16.3	3.2	0.74	2.4	2.7	0.75	5.7	3.1
B	0.15	0.12	0.23	4.9	5.2	0.22	0.7	5.2	0.23	1.7	5.2

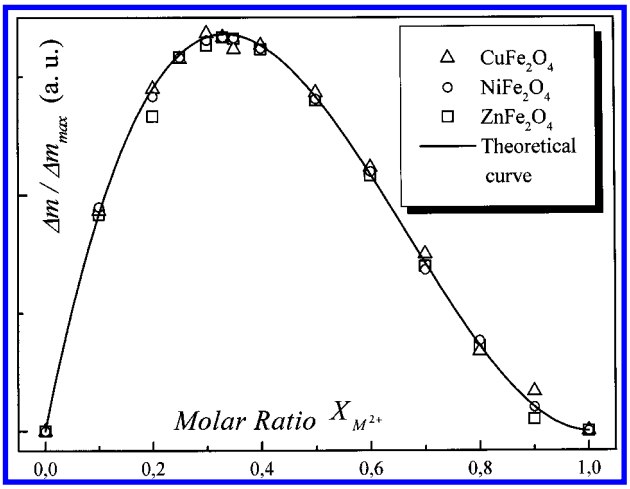

Figure 2. Normalized mass variation $\Delta m/\Delta m_{max}$ or magnetic material yield as a function of the divalent metal molar ratio, $X_{M^{2+}}$.

E. Magnetization Measurements. Moreover, to characterize the magnetic behavior of our ferrofluid samples, we measured the magnetization as a function of the applied magnetic field at 300 K using a Foner's device.[18]The experimental setup has been described elsewhere.[19] The magnetization measurements are obtained by detecting with a lock-in amplifier, and the alternating current is produced inside a small coil by the vibrations under the applied field of the ferrofluid sample linked to a vibrator.

Results and Discussion

A. Synthesis Characterization. *Titrations.* Table 1 gives the concentration, the ionic strength, the volume fraction, and the mean particle−particle distance for all the samples investigated in this work. The concentration values have been chosen in order to perform magnetization measurements on sufficiently dilute samples where the interparticle interactions can be considered as negligible.

Magnetic Material Yield. We show in Figure 2 the variations of the normalized value of the magnetic material yield as a function of the divalent metal molar ratio. Since the equilibrium constant K_f of the schematic reaction [eq 1] is generally very large (the precipitate is quite insoluble), the equilibrium lies far toward the right, and the magnetic material yield is then directly proportional to the MFe_2O_4 concentration

$$\Delta m = \alpha_M[MFe_2O_4] \quad (2)$$

where α_M mainly depends on the particle size and on the material magnetization. Then, using both the expressions of K_f and the divalent metal molar ratio, $X_{M^{2+}} = [M^{2+}]/[M^{2+} + Fe^{3+}]$, one can write the magnetic material yield as

$$\Delta m = \alpha_M K_f[M^{2+} + Fe^{3+}]^3[X^3_{M^{2+}} - 2X^2_{M^{2+}} + X_{M^{2+}}] \quad (3)$$

This last result shows, at least from a theoretical point of view, that the best value of the divalent metal molar ratio which leads to a maximum magnetic material yield corresponds to that provided by the exact ferrite stoichiometry with a value of $X_{M^{2+}}$ equal to 0.33. Moreover, as displayed in Figure 2, our measurements realized for all the synthesized nanostructured material shows a very good agreement with the theoretical curve. We can therefore conclude that the composition of all our synthesized ferrite nanoparticles perfectly respects the stoichiometric chemical formula MFe_2O_4.

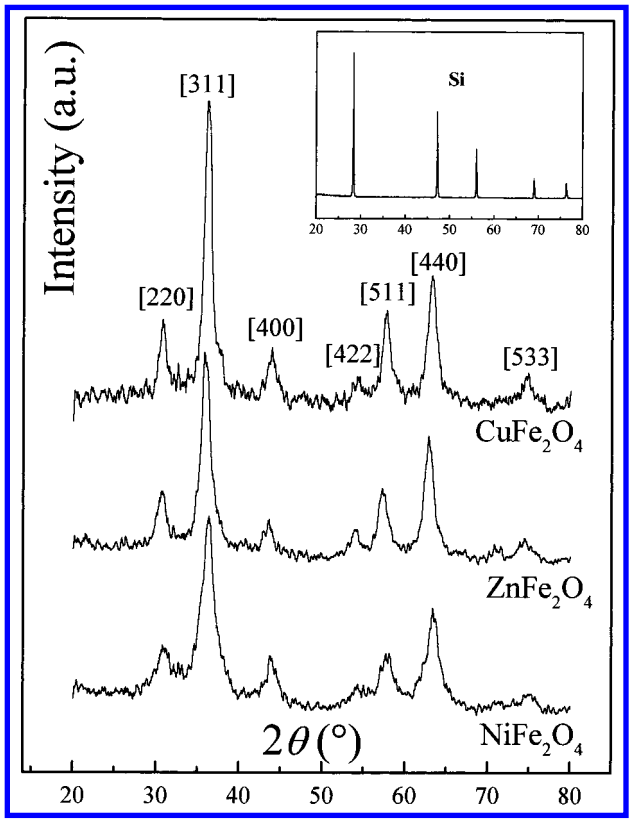

Figure 3. X-ray powder diffractograms of nickel, copper, and zinc ferrite nanoparticles. The intensity of the diffracted beams is plotted as a function of the scattering angle, 2θ, in deg. The inset displays the diffractogram obtained from a Si standard monocrystal.

TABLE 2: Nickel, Copper, and Zinc Ferrite Cubic Cells Deduced from the Analysis of X-ray Diffraction Patterns (a_{exp}), Corresponding ASTM Values (a_{ASTM}), and Mean Particle Diameter Obtained Using the Scherrer Equation (D_{XR})

	a_{exp} (nm)	a_{ASTM} (nm)	D_{XR} (nm)
$NiFe_2O_4$	0.828	0.834	4.4
$CuFe_2O_4$	0.829	0.835	8.4
$ZnFe_2O_4$	0.840	0.844	6.3

B. Structural Characterization and Particle Size Determination Using X-Ray Diffraction Experiments. The obtained X-ray diffraction spectra are displayed in Figure 3. Using the well-known Bragg law, we can index several lines and correspond them to the characteristic interplanar spacing [220], [311], [400], [422], [511], [440], and [533] of the spinel structure. Moreover, Table 2 gives for the three kinds of ferrite

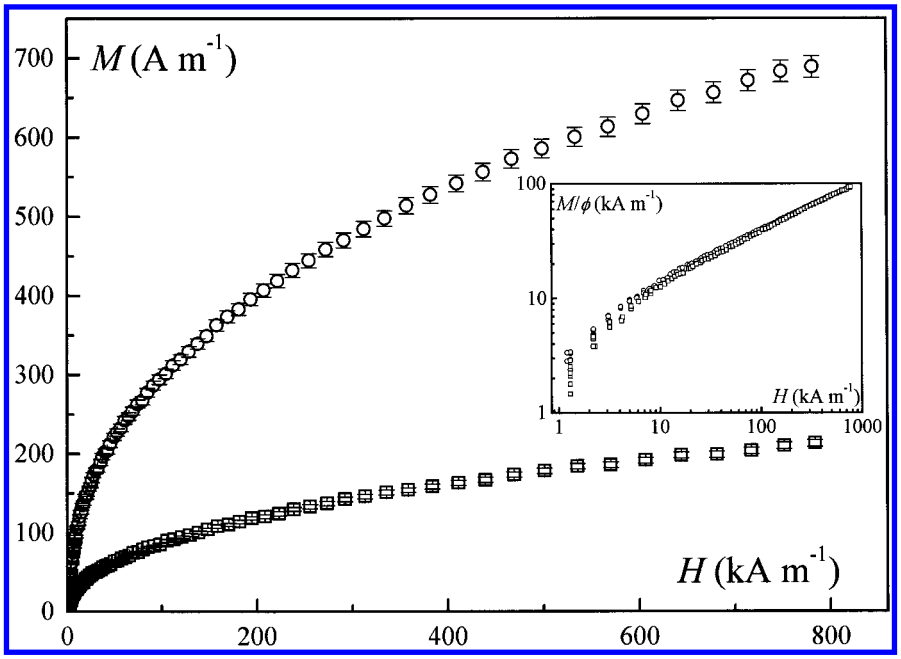

Figure 4. Magnetization M of the nickel ferrite samples (○, $\phi = 0.75\%$; □, $\phi = 0.23\%$) as a function of the applied magnetic field H in a linear representation. The inset displays in a log−log representation the normalized magnetization M/ϕ of the same samples.

samples the cubic lattice parameters we can deduce from our results, and it shows that they are in good agreement with ASTM values.[20]

From the inset of Figure 3, which displays the diffraction pattern of a Si standard monocrystal, one can see that the broadening of the ferrites diffractogram peaks can only be due to the finite dimension of the crystal (polycrystalline samples). Then, according to the Scherrer equation,[21] the roughly spherical particles size is related to the width of the diffracted beams. Using the full width at half-maximum of the most intense X-ray peak, which corresponds to the [311] one,[22] it gives in the case of our samples the nanoparticles mean diameters listed in Table 2.

C. Magnetization Measurements. The magnetic behavior of magnetic fluids results from the ultrastable suspension of single domain magnetic nanoparticles, each one bearing a permanent magnetic moment μ of a few 10^4 μ_B,[23] μ_B being the Bohr's magneton. At 300 K and for enough dilute solutions (for a volumic fraction $\phi < 2\%$), the magnetization curve reflects the orientational effect of an external magnetic field H on an ensemble of noninteracting magnetic nanoparticles which are free to rotate in the solvent. Due to such rotational degrees of freedom in a liquid carrier, the ferrofluid response to an applied field is always superparamagnetic. The orientation distribution of the magnetic moments results from a balance between the magnetic energy of the particles μH and their thermal one k_BT, k_B and T being the Boltzmann constant and the temperature, respectively. For a monodisperse solution, the magnetization is therefore well-described by a first Langevin law (L_1). Nevertheless, since the magnetic fluids are always polydisperse, the size distribution must be taken into account by considering a volume-weighted superposition of the contributions of all different particle volumes. Then, the normalized magnetization can be writen as[24,25]

$$\frac{M(H)}{m_S\phi} = \frac{\int_0^\infty D^3 L_1[\xi(D)]P(D)\,\mathrm{d}D}{\int_0^\infty D^3 P(D)\,\mathrm{d}D} \qquad (4)$$

where $\xi = \mu H/k_BT$ is the Langevin parameter, $L_1(\xi) = \coth \xi - 1/\xi$ is the first Langevin function, and the saturation value of the solution magnetization is given by $M_{sat} = m_S\phi$, m_S being the saturation magnetization of the magnetic particle and ϕ the volume fraction of the magnetic material in solution. The particles diameters distribution is generally well described by a log-normal law

$$P(D) = \frac{1}{\sqrt{2\pi}D\sigma}\exp\left[-\frac{\ln^2(D/D_0)}{2\sigma^2}\right] \qquad (5)$$

where D is the particle diameter, σ the standard deviation, and D_0 the mean value of D. The curve $M(H)/M_{sat}$ therefore reduces to a function of two parameters D_0 and σ if m_S is known. Such a model well works for magnetic fluid solutions based on typical 10 nm sized γ-Fe_2O_3 nanoparticles at 300 K, assuming for the nanomaterial a magnetization on the order of 75% of the bulk one.[25] In the case of our new synthesized nanoparticles, the nanomaterial magnetization m_S is not well-known. However, in the limit of high fields, the solution magnetization can be linearly written as a function of $1/H$, and it therefore allows a simple estimation of m_S.[26] Moreover, in the limit of low fields, the solution magnetization is proportional to the applied field. Thus, one can also obtain the size distribution parameters D_0 and σ using both the limits of low and high fields. A crossing of these results with those obtained by using the whole magnetization curve allows[24−26] a good determination of the nanoparticle size and the polydispersion.

Figures 4−6 show the magnetization curves obtained at 300 K for the three kinds of investigated magnetic fluids described in Table 1. From a qualitative point of view, all our samples exhibit the same behavior: at zero field, the magnetization is zero; as the applied field increases, the magnetization increases too, and no hysteresis is observed in the investigated range of field. Such superparamagnetic properties confirm the existence of an ordered magnetic core and the rotation of the associated core magnetic moment in the presence of an applied field. Moreover, as it can be seen on the insets of Figures 4−6, the magnetization is proportional to the volume fraction ϕ of nanomaterial showing, as expected for the values of ϕ used in

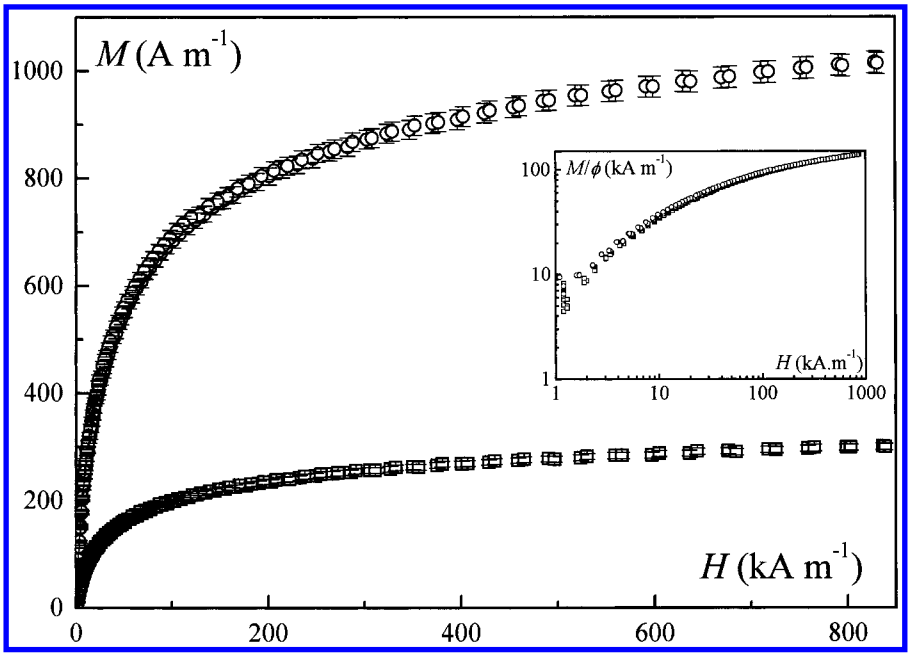

Figure 5. Magnetization M and normalized magnetization M/ϕ (inset) of the copper ferrite samples as a function of the applied magnetic field H (○, $\phi = 0.74\%$; □, $\phi = 0.22\%$).

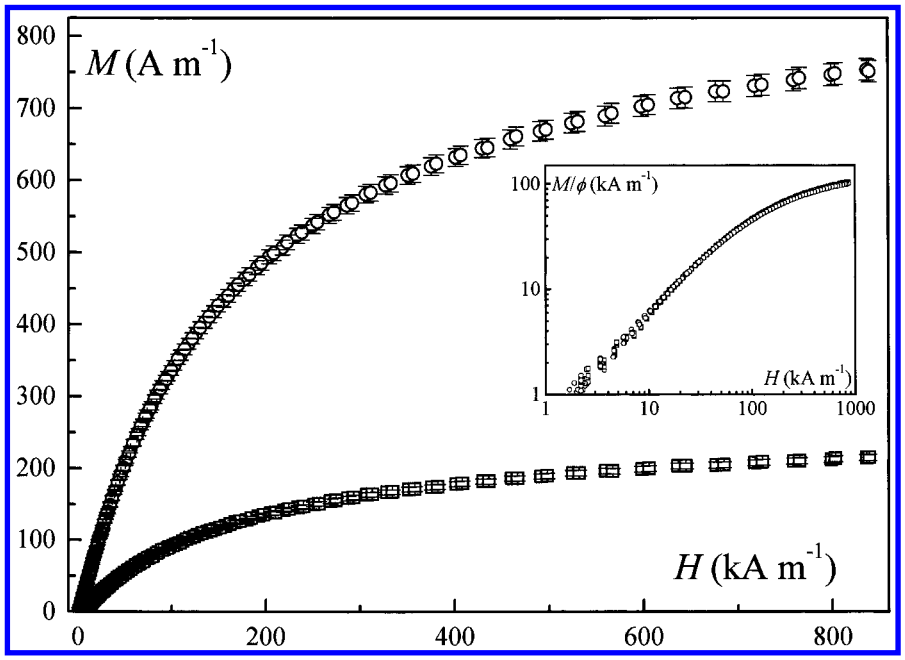

Figure 6. Magnetization M and normalized magnetization M/ϕ (inset) of the zinc ferrite samples as a function of the applied magnetic field H (○, $\phi = 0.76\%$; □, $\phi = 0.24\%$).

our experiments that, from a magnetic point of view, particle−particle interactions can be considered as negligible.

Nevertheless, comparing the results for our three kinds of samples, one can easily note that magnetic fluids based on nickel ferrite nanoparticles do not reach the saturation at our maximum field value (about 900 kA m^{-1}). Indeed, the corresponding value of the magnetization is equal to 92 ± 2 kA m^{-1} (see Figure 4 and Table 4), which is only about one-third of the bulk value. Such a result has very recently been related to the existence of a strong surface magnetism,[27] which would find its origin in the small size of the particles coupled to the nickel ferrite crystalline structure.[19] Furthermore, previous works[28] have shown that ball-milled nickel ferrite particles also exhibit anomalous magnetic behavior associated with the existence of a surface layer of disordered spins. A precise analysis carried out with our same Ni-based samples taking into account one standard contribution arising from the magnetic monodomain ordered core, which follows one Langevin formalism and another associated with a disordered surface layer, gives a magnetic size of 4.2 nm and a standard deviation of 0.4, very closed to the electronic microscopy and X-ray characterization.[6,27]

On the contrary, the magnetization of magnetic fluids based on $CuFe_2O_4$ and $ZnFe_2O_4$ nanoparticles tend toward and nearly reach the saturation. To determine their saturation behaviors, we exhibited the data in Figures 7 and 8 in logarithmic coordinates where the full line is the result of a best fit obtained by using eqs 4 and 5. The insets a of both Figures 7 and 8 present, in linear coordinates, the high-field data (H > 500 kA m^{-1}) in such a manner that m_S is determined by the value of

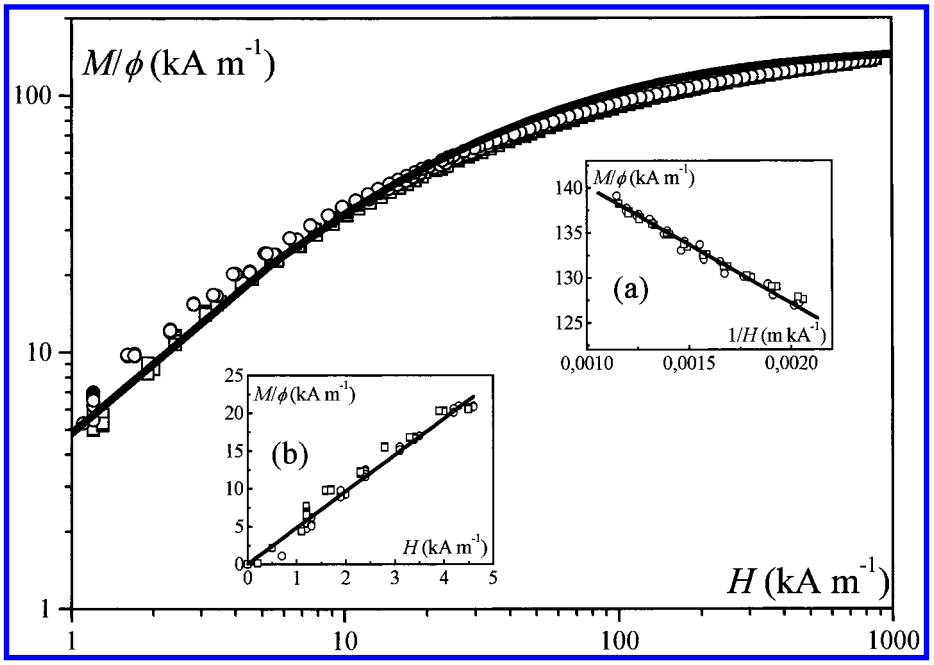

Figure 7. Log-log representation of the normalized magnetization M/ϕ of Cu-based samples as a function of the applied magnetic field H. The full line is the best fit obtained by using the Langevin formalism coupled with a log−normal distribution of diameters D of eq 4. High-field (inset a) and low-field (inset b) analyses (see Table 4 for the resulting parameters size distribution).

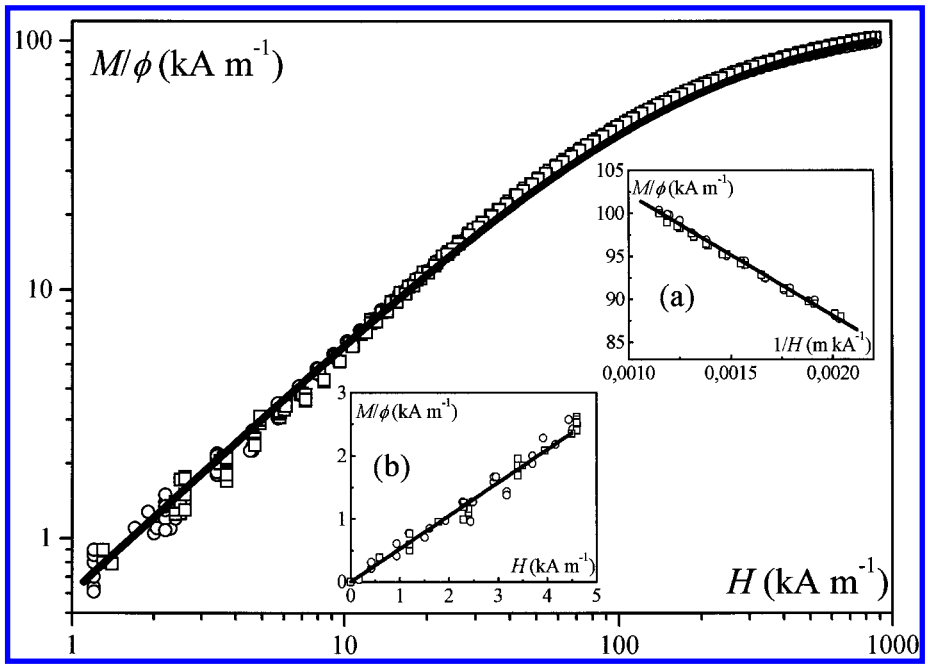

Figure 8. Log−log representation of the normalized magnetization M/ϕ of Zn-based samples as a function of the applied magnetic field H. The full line is the best fit using eq 4. High-field (inset a) and low-field (inset b) analyses (see Table 4 for the resulting parameters size distribution).

TABLE 3: Mean Nanoparticles Diameter Deduced from the Low Field Analysis (D_0^{LF}), from the High Field Analysis (D_0^{HF}), and from the Whole Magnetization Curve (D_0), Standard Deviation (σ), and Corresponding Most Probable Nanoparticles Diameter (D_{mp}) of Zinc- and Copper-Based Samples

	D_0^{LF} (nm)	D_0^{HF} (nm)	D_0 (nm)	σ	D_{mp} (nm)
$CuFe_2O_4$	7.1	6.2	6.0	0.45	4.9
$ZnFe_2O_4$	6.1	5.8	5.9	0.3	5.4

M/ϕ when $1/H$ tends toward zero. Moreover, in the insets b, the low field data are plotted in linear coordinates and show that in the low-field region ($H < 50$ kA m^{-1}), the solution magnetization $M(H)$ is actually proportional with H. Then for both samples, the solution magnetization follows closely the Langevin model, and one can accurately determine the particle diameter (magnetic size) and the standard deviation of the size distribution.[24−26] A qualitatively significant fact is that in both cases, at high fields, the magnetization does follow the linear $1/H$ law. In such a context, the analysis of our magnetization curves gives the results summarized in Table 3, where we compare D_0, the mean value of D deduced from the whole curve, with D_0^{LF} and D_0^{HF}, the values obtained from the low-field and high-field analyses, respectively. Table 3 also gives the standard deviation σ and the deduced most probable diameter $D_{mp} = D_0 e^{-\sigma^2}$. In both cases, the sizes determined by X-ray diffraction experiments (see Table 2) and those obtained by fitting the magnetization curves are well comparable. In the case of Cu-based samples, the difference between the values is larger due

TABLE 4: Saturation Magnetizations, with Their Relevant References, of Some Bulk Ferrite Materials and Corresponding Ferrite Nanoparticles (coprecipitation method)

	γ-Fe_2O_3[25]	$CoFe_2O_4$[8]	$MnFe_2O_4$[8]	$NiFe_2O_4$[27]	$CuFe_2O_4$[23]	$ZnFe_2O_4$[29]
m_S (bulk)/kA m^{-1}	360	422	386	270	135	13.5[b]
m_S (nanomaterial)/kA m^{-1}	270	305	261	270[c]	153 ± 20	122 ± 16
M_{max}/ϕ (EDL-MF)/kA m^{-1}	–	–	–	92 ± 2	138 ± 3	99 ± 2

[a] The latter value is obtained by the analysis of the magnetization curves of ferrofluid solutions. In the case of our samples, we also give the value reached by the solution magnetization (M_{max}/ϕ) at our maximum field value. [b] In this case, the given value of m_S was obtained for particles of 96 nm.[29] [c] Value used in the core−shell model.[27]

to the quite broad size distribution ($\sigma = 0.45$) when compared to Zn-based ones ($\sigma = 0.30$) and is directly related with the synthesis process.

Table 4 summarizes magnetization values of bulk ferrite materials,[23] of corresponding ferrite nanoparticles, all obtained by the same coprecipitation method, and, in the case of our three kind of samples, the values reached by the solution magnetization M_{max}/ϕ at our maximum field value. As expected, the saturation magnetization of our zinc and copper ferrites nanoparticles is about two times smaller when compared to that of maghemite,[25] cobalt,[8] and manganese[8] ferrites nanoparticles. Moreover, for Cu-based samples, the value of M_{max}/ϕ is about 90% of the m_S value used in the calculated magnetization, showing, as previously commented, that the solution almost saturates. In the case of Zn-based samples, M_{max}/ϕ is on the order of 80% of m_S, and the saturation of the solution magnetization is less fully achieved, probably due to the reduced size of zinc ferrite nanoparticles. However, both values correspond to a high magnetization when compared to the measured one, about 13.5 kA m^{-1} for 96 nm sized $ZnFe_2O_4$ particles.[29] It is well-known that zinc ferrite belongs to the class of normal spinels with tetrahedral sites (A sites) exclusively occupied by Zn^{2+} ions of zero moment and octahedral ones (B sites) by Fe^{3+} ions. Due to the B−B interaction, the Fe^{3+} ions tend to have antiparallel moments, so Zn-ferrite is described in the literature as an anomalous antiferromagnetic material with a Néel temperature on the order of 10 K.[23] Above this temperature, it becomes paramagnetic. However, there have been numerous reports indicating anomalies in the magnetic properties of zinc ferrite.[30,31] Moreover, it has been shown that $ZnFe_2O_4$ nanoparticles obtained by coprecipitation exhibit high magnetization even at room temperature (300 K), and it was found that this saturation magnetization increases with decreasing particles size.[32] As an example, the magnetization of Zn-based particle with a mean diameter of 8 nm is about 135 kA m^{-1} at 300 K for an applied magnetic field of 1500 kA m^{-1}.[33] Such a high magnetization was attributed to superexchange interactions between octahedral and tetrahedral Fe^{3+} ions induced by cations redistribution between A and B sites.[34] In our case, the value found for an applied field of 900 kA m^{-1}, equal to 99 ± 2 kA m^{-1}, and the value used in our calculations, equal to 122 ± 16 kA m^{-1}, show that such a redistribution seems to occur in our synthesized zinc ferrite nanoparticles. In the case of Cu-based samples, the value of m_S used in our calculations, equal to 153 ± 20 kA m^{-1}, is larger than the bulk value and could also be due to cation redistribution. In the ideal $CuFe_2O_4$ inverse spinel structure, the eight divalent ions (Cu^{2+}) occupy the B sites, and because a relatively small energy difference exists between Cu^{2+} ions in the A and B sites,[35] cation redistribution is possible. As an example, a single Cu^{2+} ion per unit cell on A site doubles the magnetization.[36] Moreover, a saturation magnetization equal to 164 kA m^{-1} in 6 nm sized ball-milled $CuFe_2O_4$ nanoparticles has been recently measured, and such a value has been attributed to cation redistribution between A and B sites. Nevertheless, in our two kinds of synthesized nanoparticles, further investigations, using for example Mossbauer spectroscopy, are necessary for any conclusions.

Conclusion

For the first time, magnetic fluids based on copper, nickel and zinc ferrites nanostructures have been successfully synthesized, a result which could offer a new way for biological applications. The chemical composition of our nanoparticles has been checked, and it corresponds to the ferrite stoichiometry. The best magnetic material yield corresponds to the initial stoichiometric molar ratio in divalent metal. The crystallographic structure has been identified as spinel-type. Using magnetization curves, we determined the parameters of the size distribution, and the obtained particles diameters are comparable to those given by the analysis of X-ray diffraction patterns. To further understand the magnetic behavior of our synthesized magnetic fluids, it would be of great interest to elaborate a procedure to control the particles size as well as to improve their polydispersity. In future, it will be also necessary to investigate a possible cation redistribution in our three kinds of nanoparticles as well as the magnetooptical properties of copper- and zinc-based samples.

Acknowledgment. We would like to thank Dr. E. Hasmonay (Paris) for the magnetization measurements, Dr. R. Itri (São Paulo) for the X-ray measurements, and Dr. Perzynski for very helpful discussions. We also thank the Brazilian organizations, FAP-DF, CAPES, and CNPq-PADCT for their financial support.

References and Notes

(1) Berkovsky, B. Ed. In *Magnetic Fluids and Applications Handbook*; Begell: New York, 1996.
(2) Tourinho, F. A.; Depeyrot, J.; da Silva, G. J.; Lara, M. C. F. L. *Braz. J. Phys.* **1998**, *28*, 413.
(3) Bacri, J.-C.; Perzynski, R.; Salin, D.; Cabuil, V.; Massart, R. *J. Magn. Magn. Mater.* **1990**, *85*, 27.
(4) Häfeli, U., Schüt, W., Teller, J., Zborowski, M., Eds. In *Scientific and Clinical Applications of Magnetic Carriers*; Plenum Press: New York, 1997.
(5) Häfeli, U.; Zborowski, M. *J. Magn. Magn. Mater.* **1999**, *194*.
(6) Hasmonay, E.; Depeyrot, J.; Sousa, M. H.; Tourinho, F. A.; Bacri, J.-C.; Perzynski, R. *J. Magn. Magn. Mater.* **1999**, *201*, 195.
(7) Wolhfarth, E. P. *Ferromagnetic Materials*; North-Holland: Amsterdam, 1982; Vol. 2.
(8) Tourinho, F. A.; Franck, R.; Massart, R.; Perzynski, R. *Prog. Colloid Polym. Sci.* **1989**, *79*, 128.
(9) Massart, R.; Roger, J.; Cabuil, V. *Braz. J. of Phys.* **1995**, *25*, 135.
(10) Massart, R.; Brevet, F. 7918842, 1979. U.S. Patent 4329241, 1982.
(11) Berkovsky, B. *Thermomechanics of Magnetic Fluids - Theory and Applications*; Hemisphere Publishing Corporation: Washington, DC, 1977.
(12) Pascal, P. *Nouveau Traité de Chimie Minérale*; Masson et Cie. Éditeurs: Paris, 1967; Tome XVII ,p 702.
(13) Hunter, R. J. *Foundations of Colloid Science*; Oxford Science Publications: Oxford, 1986; Vol. 1, p 13.
(14) Tourinho, F. A.; Franck, R.; Massart, R. *J. Mater. Sci.* **1990**, *25*, 3249.
(15) Sousa, M. H.; Tourinho, F. A.; Rubim, J. C. *J. Raman Spectrosc.* **2000**, *31*, 185.
(16) Vosburgh, W. C.; Cooper, G. R. *J. Am. Chem. Soc.* **1941**, *63*, 437.
(17) Hatfield, W. E. *Magnetic Measurements*; Oxford University Press: Oxford, 1987.

(18) Foner, S. *Rev. Sci. Instrum.* **1959**, *30*, 548.
(19) Hasmonay, E. Ph.D. Thesis, Université Pierre et Marie Curie, Paris, France, 1998.
(20) ASTM n° 10-0325 ($NiFe_2O_4$), 25-0283 ($CuFe_2O_4$), and 22-1012 ($ZnFe_2O_4$).
(21) Hammond, C. *The Basics of Crystallography and Diffraction*; Oxford University Press: Oxford, 1997; p 145.
(22) Amaral, L. Q.; Tourinho, F. A. *Braz. J. Phys*. **1995**, *25*, 142.
(23) Cullity, B. D. *Introduction to Magnetic Materials*; Addison-Wesley: Reading, MA, 1972; p 188.
(24) Chantrell, R. W.; Popplewell, J.; Charles, S. W. *Physica* **1977**, *86*, 1421.
(25) Bacri, J.-C.; Perzynski, R.; Salin, D.; Cabuil, V.; Massart, R. *J. Magn. Magn. Mater.* **1986**, *62*, 36.
(26) Chantrell, R. W.; Popplewell, J.; Charles, S. W. *IEEE Trans. Magn.* **1978**, *14*, 975.
(27) Hasmonay, E.; Depeyrot, J.; Sousa, M. H.; Tourinho, F. A.; Bacri, J.-C.; Perzynski, R.; Raikher, Yu. L.; Rosenman, I. *J. Appl. Phys.* **2000**, *88*, 6628.
(28) Kodama, R. H.; Berkowitz, A. E.; McNiff, E. J., Jr.; Foner, S. *Phys. Rev. Lett.* **1996**, *77*, 394.
(29) Kamiyama, T.; Haneda, K.; Sato, T.; Ikeda, S.; Asano, H. *Solid State Commun.* **1992**, *81*, 563.
(30) Lotgering, F. K. *J. Phys. Chem. Solids* **1966**, *27*, 139.
(31) Brockhouse, B. N.; Corliss, L. M.; Hastings, J. M. *Phys. Rev.* **1955**, *98*, 1721.
(32) Sato, T.; Haneda, K.; Seki, M.; Iijima, T. *Appl. Phys*. **1990**, *A50*, 13.
(33) Sato, T.; Haneda, K.; Iijima, T.; Seki, M. *Ferrites*; Proceedings from the 6th International Conference on Ferrites; The Japan Society of Powder and Powder Metallurgy: Tokyo, 1992; p 984.
(34) Anantharaman, M. R.; Jagatheesan, S.; Malini, K. A.; Sindhu, S.; Narayanasamy, A.; Chinnasamy, C. N.; Jacobs, J. P.; Reijne, S.; Seshan, K.; Smits, R. H. H.; Brongersma, H. H. *J. Magn. Magn. Mater.* **1998**, *189*, 83.
(35) Alcock, C. B.; Jacob, K. T. *Metall. Trans.* **1975**, *B 6*, 215.
(36) Goya, G. F.; Rechenberg, H. R.; Jiang, J. Z. *J. Appl. Phys.* **1998**, *84*, 1101.